Stability of out-of-phase solitons and laser pulse self-compression in active multicore fibers

A. A. Balakin,* A. G. Litvak, and S. A. Skobelev
Institute of Applied Physics of the Russian Academy of Sciences, 603950 Nizhniy Novgorod, Russia

(Received 13 September 2019; published 15 November 2019)

An out-of-phase soliton distribution of the wave field is found for a multicore fiber (MCF) from an even number of cores located in a ring. Its stability is proved with respect both to small wave-field perturbations, including azimuthal ones, and to small deformations of the MCF structure. As an example of using this soliton distribution, the problem of laser pulse compression in an active MCF is studied. The optimal fiber parameters, the minimum duration of the output pulse, and the compression length are found, and they are in good agreement with the results of numerical simulation. In order to achieve high energies in the output laser pulse, the requirements for MCF deformations are determined.

DOI: 10.1103/PhysRevA.100.053834

I. INTRODUCTION

Successful development of fiber-optic technologies in recent decades has stimulated study of the possibility of replacing high-power solid-state lasers with equivalent laser systems based on fiber components, which can fundamentally change the attractiveness of relevant applied developments. This is due to the small sizes of the fiber laser system, the ease of controlling them, and the reliability and stability of their operation. In particular, the use of an array of independent active light guides is proposed as a promising method for producing laser pulses with an extremely high power level [1,2]. The maximum achievable radiation power in each fiber is limited, but the total power can be arbitrarily large in the case of coherent summation of pulses from many fibers. One of the difficulties of this approach is the high sensitivity of the method of coherent field summation to various disturbing factors. It is necessary to maintain a constant phase difference between laser channels under conditions of random variations in the radiation phase in each channel. Recent work [3–5] has demonstrated experimentally the possibility of synchronizing laser radiation at the output of a number of independent light guides. At this, only eight light guides can be synchronized for intense wave packets.

Successful development of technologies for manufacturing multicore fibers (MCFs), which consist of identical weakly coupled optical cores located equidistantly, stimulates studies focused on the possibility of coherent propagation of laser radiation with a total power noticeably greater than that transmittable in a single-core optical fiber. Using MCFs allows one to split the total high power into cores with a power below any unwanted nonlinear effects that result in fiber damage. In other words, laser beams in each core can be safely transported below the threshold of harmful nonlinear effects, while the total coherent power can be very high. This stimulated the study of nonlinear wave processes in spatially periodic media being sets of a large number of weakly coupled optical cores.

Unfortunately, these expectations have failed. As shown by theoretical and experimental studies [6–10], such systems have their own critical power or energy at which self-focusing of the quasihomogeneous distribution of the discrete wave field occurs and the field disintegrates into a set of incoherent structures [10]. Despite this, a number of interesting results were obtained in this direction related to studying the possibilities of generating a supercontinuum [11,12], decreasing the duration of laser pulses [8–10,13–19], controlling the structure of the wave field [20–26], and producing light bullets [27–32]. The presence of a discrete critical power or energy leads to the fact that the power or energy of the laser radiation used is also limited by the destruction threshold or self-focusing in a separate core.

Recently, the research focus has shifted to MCFs with a small number of cores, e.g., MCFs consisting of a central core and an even number ($2N$) of cores located in a ring [17–22]. In such MCFs, stable inhomogeneous stationary nonlinear wave-field distributions with a total power much larger than the critical self-focusing power in continuous media were found [22]. This includes both the well-known solution localized in one core and solutions which use all cores ($\pm$ mode; where the phase differs by π in neighboring cores), half of them ("crown"-like distribution, which has the form of in-phase maxima through the core), or only several optical cores (mirror-symmetric distributions). In the case of the $\pm$ mode, the total radiation power can be many ($2N$) times higher than the critical self-focusing power in a continuous medium.

These successful efforts motivate the search for stable spatiotemporal soliton solutions for the purpose of coherent propagation of unchanged laser pulses in all available cores of such MCFs. The total energy of such a nonlinear structure can significantly exceed the energy of the nonlinear Schrödinger equation (NSE) soliton in a single core. The existence of these nonlinear solutions allows us to easily generalize the well-known methods of laser pulse compression in a single core to the case of the MCF, i.e., to take a significant step in solving the problem of formation of high-energy (sub-μJ), short-duration laser pulses in systems based entirely on the fiber design. Note that in the case of a single-core fiber in the

*balakin@appl.sci-nnov.ru

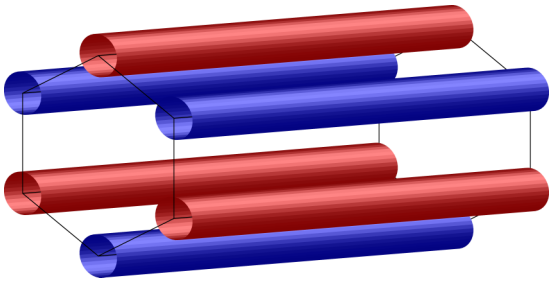

FIG. 1. Schematic of the considered MCF with cores arranged in a ring. Color reflects the out-of-phase distribution of the wave field $u_n \propto (-1)^n$.

region of anomalous group velocity dispersion (in the region of existence of NSE solitons), many schemes for decreasing the wave-packet duration are well developed; among them are the use of (i) a high-order soliton [33–35], (ii) adiabatic change in the parameters of a solitonlike laser pulse in a waveguide system with a monotonically decreasing dispersion [35,36], and (iii) adiabatic change in the parameters of a solitonlike laser pulse in a medium with amplification [37,38].

The goal of this work is to study the existence and stability of the spatiotemporal soliton in an MCF being a ring of $2N$ identical weakly coupled cores (see Fig. 1), with the aim of the possibility of coherent propagation of unchanged laser pulses in all available MCF cores. As an example of the use of this soliton, we analyze the adiabatic decrease in the soliton duration in the active MCF with a finite Gaussian amplification band under the condition of a nonstationary nonlinear response of the medium. Based on the variational approach, the minimum duration and, accordingly, the maximum energy of the laser pulse were determined. The possibility of generating a laser pulse of 55-fs duration with a sub-μJ level of energy at the MCF output at a length of 3 m and at a wavelength of 2 μm doped with thulium was demonstrated. The requirements for maximal MCF deformations and the spread of the gain in the cores for achievement of high energies in the output laser pulse are determined.

The paper is organized as follows. In Sec. II, the basic equations are formulated. In Sec. III, the spatiotemporal soliton in the passive MCF is found, and its stability with respect to azimuthal perturbations is analyzed. In Sec. IV, we consider the stability of the solution found with respect to small deformations of the MCF structure and the spread of the gain across the cores. In Sec. V, we perform a qualitative analysis of the adiabatic decrease in the duration of the found spatiotemporal soliton in the active MCF with a finite Gaussian gain band allowing for nonstationarity of the nonlinear response. Section VI presents the results of a numerical simulation of the laser pulse self-compression in a silica MCF made up of six cores doped with thullium. In the Conclusion (Sec. VII), the main results of the work are formulated.

II. FORMULATION OF THE PROBLEM

Let us consider the self-action of subpicosecond laser pulses in an active multicore fiber with a finite-gain bandwidth taking into account the instantaneous electron (Kerr) and delayed molecular (Raman) nonlinearities. Next, we consider an MCF made of an even ($2N$) number of cores arranged in a ring. Figure 1 shows schematically an MCF with $N = 3$. The analysis is based on the standard theoretical model [6,8,10,17,23,25,39], in the framework of which it is assumed that the fundamental guided modes of the optical cores oriented parallel to the z axis are weakly coupled. In this case, the propagation of laser pulses in the MCF can be described approximately as a superposition of fundamental modes localized in each core,

$$E \simeq \sum_n E_n(z,t)\phi(x-x_n, y-y_n)e^{ik_n z - i\omega t} + \text{c.c.}, \quad (1)$$

where $\phi(x, y)$ is the structure of the lowest spatial mode in the core, and E_n is the envelope of the electric-field strength in the nth core, which slowly changes along the z axis. We assume that the central frequency of the laser pulse lies in the region of the anomalous group velocity dispersion. We neglect the gain saturation of the wave packet, since fiber laser systems have a high saturation energy. For example, the saturation energy of erbium fiber laser systems is approximately 10 μJ [40,41], and the energy of the considered laser pulses is less than 10 nJ per the core.

The evolution of the wave-field envelope in the nth core can be affected by linear dispersion and the Kerr nonlinearity of a single core, amplification in the active medium, and interaction with the nearest-neighboring cores that arises due to weak overlapping of their fundamental modes. Assuming that the cores are weakly coupled, we obtain the following system of equations for the envelope of the electric field E_n in the nth core [10,16,17,41]:

$$i\frac{\partial E_n}{\partial z} + i\frac{\partial k_n}{\partial \omega}\frac{\partial E_n}{\partial t} = \frac{\beta_n}{2}\frac{\partial^2 E_n}{\partial t^2} + \sum_{m=1}^{2N}\chi_{mn}E_m + \Gamma_n P_n^{\mathrm{NL}} + \frac{i\omega_0}{4\pi n_{0n}c}\int_{-\infty}^{+\infty} X_n(\omega)E_n(z,\omega)e^{-i\omega\tau}d\omega. \quad (2)$$

Here, the subscript n varies from 1 to $2N$, ω_0 is the carrier frequency of the laser pulse, c is the speed of light, the coefficient $\chi_{mn} = \chi_{nm}$ determines the coupling between core m and core n, $\chi_{nn} = k_n$ is the wave number in the cores, n_{0n} and Γ_n are the linear and nonlinear refractive indexes in the nth core, respectively, $X_n(\omega)$ is the imaginary part of the susceptibility in the nth core, and $\beta_n = \partial^2 k_n/\partial\omega^2$ is the group velocity dispersion in the nth core. The term P_n^{NL} takes into account the time dependence of the nonlinear response of the fiber [35,39],

$$P_n^{\mathrm{NL}} = (1-f_R)|E_n|^2E_n + f_R E_n\int_0^{\infty}|E_n(t-t')|^2 h_R(t')dt', \quad (3)$$

where f_R represents the partial contribution of the inertial Raman scattering response to nonlinear polarization. The Raman response function h_R is responsible for the Raman gain and can be determined from the experimentally measured Raman spectrum in silica fibers. The approximate analytical form of this function is as follows [35,39]:

$$h_R(t) = \frac{\tau_1^2+\tau_2^2}{\tau_1\tau_2^2}\exp(-t/\tau_2)\sin(t/\tau_1). \quad (4)$$

For silica fiber, we have $\tau_1 = 12.2$ fs, $\tau_2 = 32$ fs, and $f_R = 0.18$ [39]. When analyzing the nonlinear dynamics of laser pulses with a duration of $\tau_p \gg \tau_2$, expression (3) can be simplified:

$$P_n^{\mathrm{NL}} \approx |E_n|^2 E_n - \tau_R E_n \frac{\partial |E_n|^2}{\partial t}, \quad \tau_R = \frac{2 f_R \tau_1^2 \tau_2}{\tau_1^2 + \tau_2^2}. \tag{5}$$

We assume that all cores are the same: $\Gamma_n \equiv \Gamma$, $X = X_n$, $\chi_{nm} = \widehat{\chi}\delta_{n,m\pm1}$, $\beta_n = \beta$, $n_{0n} = n_0$. In the accompanying coordinate system moving at the group velocity of the wave packet, the system of equations (2) taking into account expression (5) can be written in dimensionless variables as follows:

$$i\frac{\partial u_n}{\partial z} = \frac{\partial^2 u_n}{\partial \tau^2} + |u_n|^2 u_n - \mu u_n \frac{\partial |u_n|^2}{\partial \tau} + \chi(u_{n+1} + u_{n-1}) + \delta h_n u_n + \frac{i}{2\pi}\int_{-\infty}^{+\infty} G(\omega) S_n(\omega) e^{-i\omega\tau} d\omega. \tag{6}$$

Here, the longitudinal coordinate $\tau = t - \frac{\partial k}{\partial \omega} z$ and the evolutionary coordinate z are normalized to the characteristic laser pulse duration τ_{in} and the corresponding dispersion length $z_0 = 2\tau_{\mathrm{in}}^2/\beta$, $u_n = e^{-ih_n z} E_n \sqrt{\Gamma z_0}$ is the complex amplitude of the envelope of the wave packet in the nth core, $h_n = k_n^{(0)} z_0$, $k_n = k_n^{(0)} + \delta k_n$, $\chi = \widehat{\chi} z_0$, $\delta h_n = \delta k_n z_0$; $S_n = \int_{-\infty}^{+\infty} u_n(\tau) e^{i\omega\tau} d\tau$ is the envelope spectrum; and $\mu = \tau_R/\tau_{\mathrm{in}}$, $G = \frac{\omega_0 z_0}{2 n_{0c}} X(\omega)$. The Gaussian distribution will be chosen as the gain profile of the active medium $G(\omega)$:

$$G(\omega) = \gamma \exp(-\omega^2/\Omega^2). \tag{7}$$

The second term in Eq. (6) describes the linear dispersion of the medium, the third term is responsible for the Kerr nonlinearity, and the fourth term is the inertia of the nonlinear response. Further terms are responsible for coupling with neighboring cores. The last term, describing the process of amplification of a laser pulse in an active medium, is represented through the spectral gain $G(\omega)$. In the case of a single-core fiber, the reduced system of equations corresponds to the well-known equation from [41].

The applicability of Eqs. (6) is limited by the approximation of the single-mode wave-field propagation in each core. It is violated when the radiation power in any of the cores $\mathcal{P}_n = |E_n|^2 \iint \phi^2 dxdy$ becomes close to the critical power of self-focusing in a homogeneous medium $\mathcal{P}_{\mathrm{cr}}$.

III. SPATIOTEMPORAL SOLITONS

A number of stable nonlinear solutions for wave beams propagating in the considered MCFs were found in [22]. The most interesting of these is the $\pm$ mode $u_n \propto (-1)^n$, which provides transportation of maximum power at a given field amplitude. Moreover, this solution is stable and exists at all amplitudes.

The generalization of the $\pm$ mode to the pulsed case is simple, since wave-field amplitudes in all cores are the same. Indeed, Eqs. (6) in the absence of amplification $G = 0$ and an inertia of nonlinear response $\mu = 0$ have a solution in the form

$$u_n(z,\tau) = (-1)^n \frac{\sqrt{2} b e^{i(2\chi - b^2)z}}{\cosh(b\tau)}. \tag{8}$$

To prove the stability of the manifold, (8), we use the *second Lyapunov method*. It says that the variety of solutions will be stable if it is possible to find the Lyapunov functional $\mathcal{F}[u]$ that satisfies the following requirements: (i) it is always positive, $\mathcal{F}[u] \geqslant 0$; (ii) the derivative is less than or equal to 0, $\frac{d}{dz}\mathcal{F} \leqslant 0$; and (iii) $\mathcal{F}[u_s] = 0$ *only* on this manifold.

The key point here is the requirement of uniqueness, $\mathcal{F}[u] = 0$, for the analyzed solution only. For example, for the nonlinear oscillator $\ddot{x} - x + x^3 = 0$, the Lyapunov functional $\mathcal{F} = (\dot{x}^2 - x^2 + x^4/2 - \mathcal{H}_0)^2$ shows the stability of the manifold of nonlinear oscillations at $\mathcal{H}_0 \neq 0$ with different initial phases. However, in the case of $\mathcal{H}_0 = 0$, it only proves the stability of *both* separatrices as a whole. Moreover, each individual separatrix (left or right) is unstable, despite the movement occurring only along individual separatrices. This reflects the presence of a stochastic layer in the small vicinity of the saddle point and separatrices, which allows a random jump from one separatrix to another.

Equations (6) with $\mu = G = 0$ preserve the Hamiltonian $\mathcal{H}$ and the energy W:

$$\mathcal{H} = \sum_{n=1}^{2N} \int_{-\infty}^{+\infty} \left[\left| \frac{\partial u_n}{\partial \tau} \right|^2 - \frac{|u_n|^4}{2} - \chi(u_n u_{n+1}^* + u_{n+1} u_n^*) \right] d\tau, \tag{9a}$$

$$W = \sum_{n=1}^{2N} \int_{-\infty}^{+\infty} |u_n|^2 d\tau. \tag{9b}$$

These are the standard Hamiltonian and total energy of the wave field in the system of weakly coupled light guides (see [28] and cited works). The Hamiltonian $\mathcal{H}$ is well suited for the role of the Lyapunov functional, but it is not formally bounded below. Indeed, an increase in the field amplitude due to a perturbation can lead to an increase in the nonlinear term and a decrease in the value of $\mathcal{H}$. Let us find the minimum of the Hamiltonian $\mathcal{H}$ in the class of functions that conserve energy using the method of indefinite Lagrange multipliers. The first variation of the functional $\mathcal{R}[u] = \mathcal{H}[u] + \lambda W[u]$ with respect to u_n^* gives the equation

$$-\frac{\partial^2 u_n}{\partial \tau^2} - |u_n|^2 u_n - \chi(u_{n+1} - 2u_n + u_{n-1}) + \lambda u_n = 0 \tag{10}$$

for the soliton manifold ($\lambda_m = \lambda - 2\chi\cos\kappa_m$)

$$u_n^{(\mathrm{m})} = e^{i\kappa_m n} \frac{\sqrt{2\lambda_m}}{\cosh\sqrt{\lambda_m}\tau}, \quad W_m = 8N\sqrt{\lambda_m}. \tag{11}$$

The Hamiltonian value for this solution is

$$\mathcal{H}_m^{\mathrm{sol}} = -16N\chi\sqrt{\lambda_m}\cos\kappa_m - \frac{8N}{3}\lambda_m^{3/2} = -2\chi W_m \cos\kappa_m - \frac{W_m^3}{192N^2}. \tag{12}$$

Then the functional

$$\mathcal{F}_m[u] = \left(\mathcal{H}[u] + \frac{W[u]^3}{192N^2} + 2\chi W[u]\cos\kappa_m \right)^2 \tag{13}$$

satisfies the conditions of $\mathcal{F}_m[u_n^{\mathrm{sol}}] \geqslant 0$ and $d\mathcal{F}_m[u]/dz = 0$. The main difficulties arise in proving the uniqueness of the functional turning to 0 only in solution (11) and nowhere else.

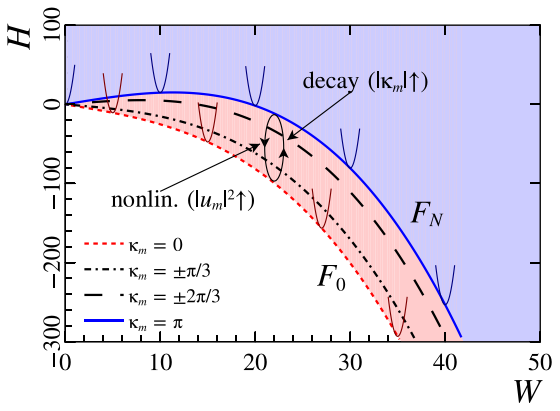

FIG. 2. Dependence, (9), of the Hamiltonian $\mathcal{H}$ on the energy W. Curves correspond to the extrema, (12), for various m values. Arrows show qualitative explanations of instability at $m = 0$.

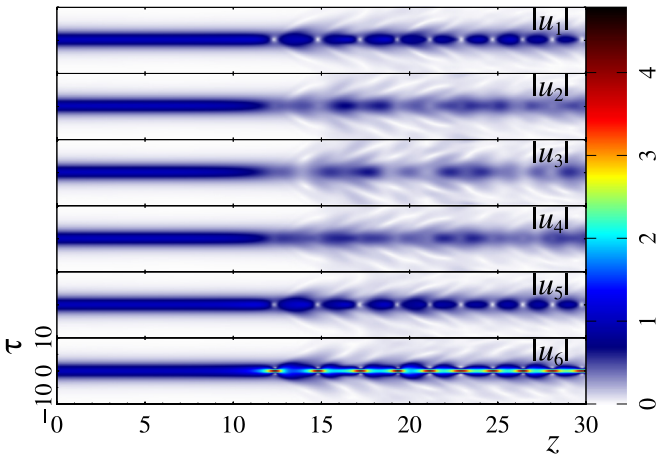

FIG. 3. Dynamics of the wave-field envelope $|u_n|$ in a six-core MCF ($N = 3$) with the coupling coefficient $\chi = 1$. The initial distribution is $u_n = \sqrt{2}b/\cosh(b\tau)$ with $b = 0.7$.

We first consider the simplest case of $N = 1$. In this case, there are only two solutions, with $\kappa_m = \pi$ (out of phase) and $\kappa_m = 0$ (in phase). Figure 2 shows the dependence of $\mathcal{H}_m^{\rm sol}$, (12), on W, which corresponds to the minimum value of the Hamiltonian $\mathcal{H}$ at a fixed energy value W. Here, the solid blue curve corresponds to the case $\kappa = \pi$, and the dashed red line corresponds to $\kappa = 0$. On these curves, the functional $\mathcal{F}$ vanishes. Recall that the quantities $\mathcal{H}$ and W are integrals of the problem. Note that the value of the Hamiltonian $\mathcal{H}_N^{\rm sol}$ in the solution at $\kappa_m = \pi$ is always greater than the value $\mathcal{H}_0^{\rm sol}$ at $\kappa_m = 0$ (see Fig. 2). If we add a small perturbation of the field to the solution $\tilde{u} = u^{(\rm m)} + \delta u$, then the resulting wave field can turn into a soliton with different parameters (λ, κ_m) and some small ripples (the variety of solutions is stable) or can fall apart completely (unstable). Note that the perturbed field corresponds to new values of the energy $W[\tilde{u}]$ and the Hamiltonian $\mathcal{H}[\tilde{u}]$.

An increase in the intensity difference in the cores for the case of the solution at $\kappa_m = 0$ leads to an increase in the nonlinear term and thereby to a decrease in the Hamiltonian $\mathcal{H}$, (9a). This change in the Hamiltonian is easily compensated by a decrease in the term that contains χ (for example, the appearance of a phase difference due to the decay to $\kappa_m = \pi$). As a result, the same values of $\mathcal{H}$ and W (that is, $\mathcal{F}_0 = 0$) correspond to different distributions. Thus, the in-phase solution is unstable and tends to beats with radiation capture in one core. On the contrary, the value of the Hamiltonian in the solution at $\kappa_m = \pi$ is always greater than its value at $\kappa_m = 0$. This means that a distribution with $\kappa_m = \pi$ cannot decay into a distribution with smaller $\kappa_m = 0$. Therefore, an increase in the nonlinear term at $\kappa_m = \pi$ cannot be compensated and leads to $\mathcal{F}_N > 0$. In other words, the values of $\mathcal{H} \neq \mathcal{H}_N^{\rm sol}$ and $W^{\rm sol}$ correspond to different distributions. Thus, the out-of-phase soliton distribution is stable.

Now, we get back to the case of $N \geqslant 2$. An increase in the number of cores leads to the appearance of additional modes at $\kappa_m = m\pi/N$. Again, it is possible to show the uniqueness of the functional $\mathcal{F}$, (13), turning to 0 only for the $\pm$ mode with $\kappa_m = \pi$ (that is, $m = N$). For all other $m \neq N$, the functional (13) can be set to 0 for $u_n \neq u_n^{(m)}$. This fact reflects the presence of filamentation instability at $\kappa_m \neq \pi$. The situation in this case is similar to the classical filamentation instability, which develops on a quasihomogeneous wave packet with constant energy and Hamiltonian integrals.

Indeed, let us investigate the obtained solution with respect to filamentation instability for $N \geqslant 2$, using a wave field with perturbations in the form

$$u_n^{(m)} = [f_m e^{i\kappa_m n} + \delta_s e^{i\lambda z + i\kappa_s n}] e^{-i(2\chi\cos\kappa_m + f_m^2)z}.$$

Assuming $|\delta_s| \ll f_m$, we get real eigenvalues

$$\lambda^2 = 4\chi[\cos\kappa_m - \cos\kappa_s]\big[\chi(\cos\kappa_m - \cos\kappa_s) - f_m^2\big]. \quad (14)$$

For $\kappa_m \neq \pi$, a stable coherent radiation propagation regime ($\lambda^2 > 0$) is realized only when the wave-field amplitude in the core is less than the critical value $f_m < f_{\rm cr}$. For example, in the case of an isotropic field distribution on the ring ($\kappa_m = 0$), the filamentation is absent only at amplitudes

$$f_0 < f_{\rm cr} = \sqrt{2\chi}\sin\frac{\pi}{2N} \underset{N\gg 1}{\approx} \frac{\pi}{N}\sqrt{\frac{\chi}{2}}. \quad (15)$$

Next, we turn to the results of numerical simulations in order to verify the above qualitative analysis of the stability of solution (11) for $\kappa_m \neq \pi$. Figure 3 shows the evolution dynamics of a laser pulse with initial isotropic ($\kappa_m = 0$) distribution $u_n = \sqrt{2}b/\cosh(b\tau)$ in a six-core MCF ($N = 3$) with the coupling coefficient $\chi = 1$ and the amplitude $b = 0.7$. With these parameters, the initial pulse amplitude is greater than the critical value ($\sqrt{2}b > f_{\rm cr} = 1/\sqrt{2}$). The results of numerical simulations confirm the instability of solution (11) at $\kappa_m = 0$. As the wave packet propagates in the medium, the radiation is captured in an arbitrary core (at $z \sim 12$). This leads to a decrease in the duration of the laser pulse by several times [17,18]. Further, complex quasiperiodic dynamics occur, similar to multisoliton dynamics in the case of a single core.

IV. RESISTANCE TO MCF DEFORMATION

The stability of the found spatiotemporal soliton, (8), with respect to small perturbations of the wave field suggests its

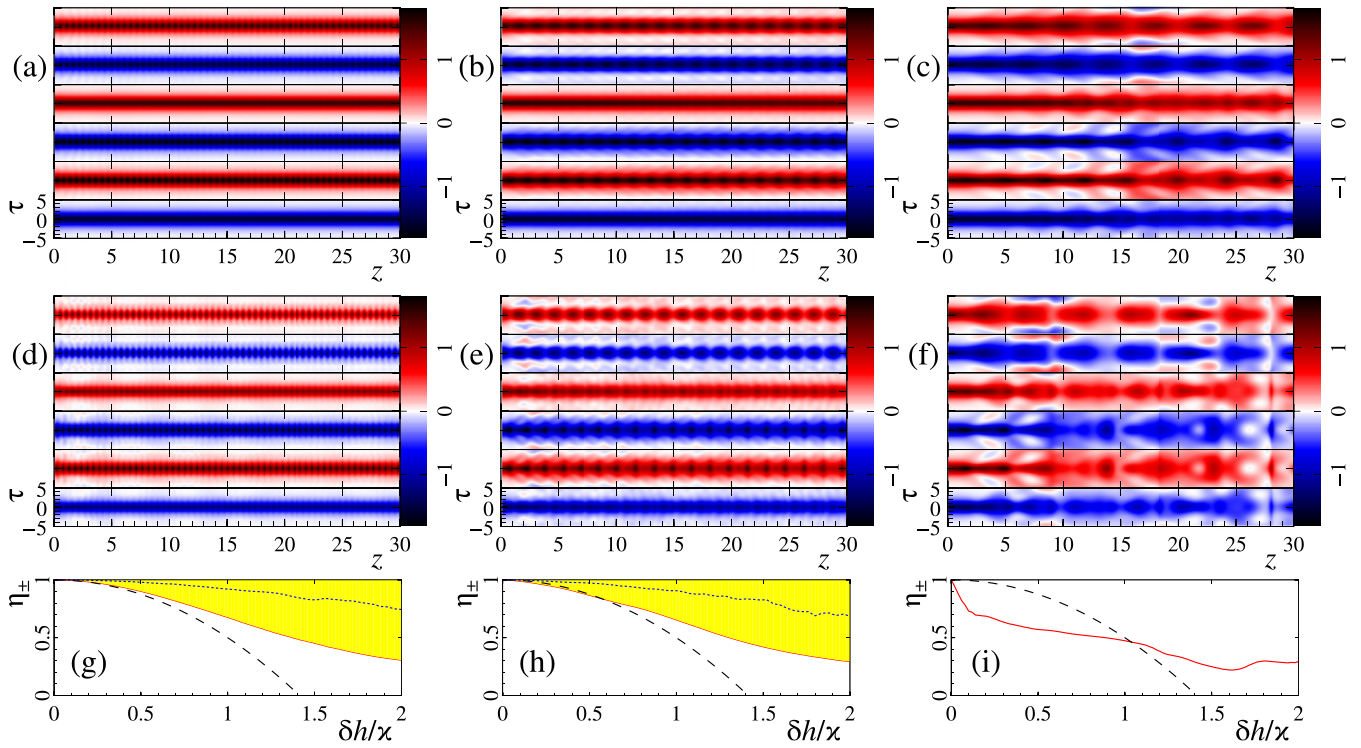

FIG. 4. Envelope dynamics of the wave field $\mathrm{Re}[u_n(z,\tau)]$ in six-core MCFs ($N=3$) in the case of fiber bending $h_n = h + \delta h \sin(\pi n/N)$ for different values of the coupling coefficient χ: (a, d, g) $\chi = 10$; (b, e, h) $\chi = 3$; and (c, f, i) $\chi = 1$. The top row corresponds to $\delta h/\chi = 0.1$; the middle row, to $\delta h/\chi = 0.3$. The spatiotemporal soliton $u_n = (-1)^n\sqrt{2}b/\cosh(b\tau)$ was injected at the MCF input with $b = 1$. (g, h, i) Dependence of the fraction of energy $\eta_\pm$ in the $\pm$ mode on the value of the parameter $\delta h/\chi$. Here, the dashed black line is the estimate, (26), found for the beam problem. The red line shows the results of numerical modeling. The yellow region represents the fraction of energy in the $\pm$ mode, when δh_n is random and lies in the range $0 \leqslant \delta h_n \leqslant \delta h$. Blue dots represent the fraction of energy in the $\pm$ mode after averaging over the ensemble.

stability with respect to small deformations of the MCF structure ($\delta h_n \neq 0$). The results of numerical modeling confirm this conclusion. As an example, consider two cases: (i) the linear gradient $\delta h_n = \delta h \sin(\pi n/N)$, and (ii) the value of δh_n is random and lies in the interval $0 \leqslant \delta h_n \leqslant \delta h$.

Figure 4 shows the results of the numerical simulation of the evolution of the wave packet, (8), in a six-core MCF ($N = 3$) for different values of the coupling coefficient χ: $\chi = 10$ [Figs. 4(a), 4(d), 4(g)]; $\chi = 3$ [Figs. 4(b), 4(e), 4(h)]; and $\chi = 1$ [Figs. 4(c), 4(f), 4(i)]. A laser pulse, (8), with $b = 1$ was injected at the input of the MCF. The top row corresponds to the case $\delta h/\chi = 0.1$; the middle row, to $\delta h/\chi = 0.3$. The gradient of the refractive index [$\delta h_n = \delta h \sin(\pi n/N)$] leads to the fact that the field distribution becomes inhomogeneous along the MCF ring. The field amplitude has maximal values in the cores, where $\delta h_n = -\delta h$ and, accordingly, minimal values at $\delta h_n = \delta h$. In Figs. 4(g)–4(i), the red line shows the dependence of the fraction of energy $\eta_\pm = 1/(1 + \delta W/W)$ in the $\pm$ mode on the modulation depth $\delta h/\chi$ for different values of the coupling coefficient χ, where $\delta W/W$ is the fraction of energy in other modes ($\kappa_m \neq \pi$). It can be seen that with an increasing depth of the modulation $\delta h/\chi$, the fraction of the energy in the $\pm$ mode decreases, obeying a parabolic law.

Figures 4(a)–4(c) show that deformations of the MCF have almost no effects on the dynamics of soliton propagation in the case of $\chi \geqslant 3$ and the modulation depth $\delta h/\chi = 0.1$. Over the entire interval of the numerical calculation, the soliton duration does not change ($z \ggg z_{\mathrm{dis}}$, where $z_{\mathrm{dis}} \simeq 1$ is the dispersion length) and the $\pm$ mode is not disturbed (the relative phase difference in neighboring cores is π). The fraction of the energy in the $\pm$ mode is $\eta_\pm \approx 0.98$. With an increasing modulation depth [see Figs. 4(d)–4(f)] of the refractive index ($\delta h/\chi = 0.3$), the temporal structure remains unchanged only at a large coupling coefficient, $\chi = 10$ [see Fig. 4(d)]. Only some beats in the amplitude with respect to z are observed. The fraction of the energy in the $\pm$ mode is $\eta_\pm \approx 0.82$. However, with the coupling coefficient $\chi = 3$ [see Fig. 4(e)], the temporal profile of pulses deteriorates. In the case of the coupling coefficient $\chi = 1$, the solution found does not hold well in the time domain [see Fig. 4(f)]. Therefore, in the case of the coupling coefficient $\chi = 10$, the deformations of the MCF do not affect the found spatiotemporal soliton essentially. For a given coupling coefficient, the coupling length $1/\chi$ is 10 times less than the dispersion length. Accordingly, the soliton manages to adapt itself every time to changes in the medium.

Results of numerical simulations demonstrate stability of the spatial distribution in the MCF within the considered parameter range (χ, $\delta h/\chi$). The relative phase difference of the field in adjacent cores is π. As noted above, the found solution, (8), is not destroyed in numerical simulation if the dispersion length is much less than the coupling length, i.e., $b^2 \ll \chi$. The result of numerical simulations for the fraction of the energy in the $\pm$ mode can be approximated by the

expression [dashed black lines in Figs. 4(g) and 4(h)]

$$\eta_{\pm} \equiv \frac{\int \left|\sum(-1)^n u_n\right|^2 d\tau}{2NW} \approx 1 - (\delta h/\chi)^2/2, \qquad (16)$$

which is the same as estimate (26) below. It shows that the perturbation energy is negligible at $\delta h \ll \chi$.

Along with this, a series of numerical calculations was performed (with approximately 1000 realizations) when the refractive index was changed randomly in the range $0 \leqslant \delta h_n \leqslant \delta h$. In this case, the $\pm$ mode was also preserved up to the coupling coefficient $\chi \geqslant 3$. In each numerical calculation, the fraction of the energy in the $\pm$ mode was random but was limited to the region shown in yellow in Figs. 4(g) and 4(h). The dashed blue line shows the fraction of energy in the $\pm$ mode averaged over the ensemble. It follows from the figure that the average fraction of energy $\eta_{\pm}$ for random perturbations δh_n is larger than that in the case of the statically bending MCF.

Thus, the found spatiotemporal soliton, (8), remains stable with respect to the MCF deformations in the case where the dispersion or nonlinear length is much greater than the coupling length, i.e., $\chi \gg b^2$. The stability estimate, (16), of the $\pm$ modes with respect to the deformation of the MCF structure ($\delta h_n \neq 0$) and the amplification distribution over the MCF cores ($\gamma_n \neq 0$) can also be obtained analytically.

The appearance of large-scale deformations, as a rule, means that all linear modes in the MCF are excited, which makes the task difficult for analytical consideration. However, if the values δh_n and $\delta\gamma_n = \gamma_n - \gamma$ are small (where $\gamma = \sum \gamma_n/2N$), the perturbations of the $\pm$ mode will remain small. If the dispersion length is much less than the average gain length ($\gamma \ll B^2$), i.e., when the amplification of a solitonlike pulse occurs in the adiabatic mode, then an approximate solution of Eq. (6) for $N \geqslant 2$ can be sought in the form

$$u_n = \sqrt{2}B\frac{(-1)^n + \delta_n}{\cosh(B\tau)} e^{2i\chi z - iB^2/2\gamma}, \quad B = b_0 e^{2\gamma z}. \qquad (17)$$

Substituting this into Eq. (6) we find, in the first order of smallness with respect to $\delta_n, \delta h_n/\chi, \delta\gamma_n/\chi \ll 1$,

$$i\partial_z \delta_n \approx \chi(\delta_{n+1} + 2\delta_n + \delta_{n-1}) + (\delta h_n + i\delta\gamma_n)(-1)^n. \qquad (18)$$

Here, we have neglected the term $4B^2\delta_n/\cosh^2(B\tau)$ due to the smallness of the coupling length compared to the dispersion length $B^2/\chi = b_0^2 e^{2\gamma z}/\chi \ll 1$ and the stability of solution (8) with respect to small wave-field perturbations (see Sec. III). Note that the stability of solution (8) to small field perturbations is also preserved in the active medium $\gamma \neq 0$ in the case $\gamma \ll B^2$. Equations (18) are a system of coupled linear oscillators, which is driven by the force $(\delta h_n + i\delta\gamma_n)(-1)^n$. Its forced (partial inhomogeneous) solution is easily found using the Fourier series expansion

$$\delta_n \approx -\frac{1}{2N}\sum_m \sum_{k\neq N} (\delta h_m + i\delta\gamma_m)\frac{(-1)^m e^{i\kappa_k(n-m)}}{4\chi\cos^2\frac{\kappa_k}{2}}. \qquad (19)$$

Typical examples of changes in the refractive index and the gain are

$$\delta h_n = \delta h \sin\frac{\pi n}{N}, \quad \delta\gamma_n = \delta\gamma \sin\frac{\pi n}{N}, \qquad (20)$$

resulting from bending of optical fibers. Here, δh and $\delta\gamma$ are the deformation amplitudes. For such disturbances, the form of the solution is much simpler:

$$\delta_n \approx -\frac{\delta h + i\delta\gamma}{4\chi\sin^2\frac{\pi}{2N}}(-1)^n \sin\frac{\pi n}{N}. \qquad (21)$$

It can be seen from the obtained formulas that the perturbations remain small ($|\delta_n| \ll 1$) in the following cases:

(a) the refractive index perturbation is small compared to the coupling coefficient,

$$\delta h_n \ll 4\chi \sin^2\frac{\pi}{2N}; \qquad (22)$$

(b) the average gain γ is small compared to the dispersion, and the coupling length is small compared to the dispersion one,

$$\gamma \ll B^2 \ll \chi; \qquad (23)$$

(c) gain perturbations are small compared to the coupling coefficient,

$$\delta\gamma \ll 4\chi \sin^2\frac{\pi}{2N}. \qquad (24)$$

Note that the energy in the perturbed part is a quantity of the second order of smallness due to the orthogonality of the perturbations and the $\pm$ mode:

$$\delta W = \sum \int \frac{|u_n|^2 - 4NB^2}{\cosh^2(B\tau)} d\tau \approx 4B\sum |\delta_n|^2. \qquad (25)$$

In the particular case of perturbations, (20), the expression for the fraction of energy in the perturbations takes a simple form:

$$\frac{\delta W}{W} \equiv 1 - \eta_{\pm} \approx \frac{(\delta h/\chi)^2 + (\delta\gamma/\chi)^2}{32\sin^4\frac{\pi}{2N}}. \qquad (26)$$

This estimate is in good agreement with the results of numerical simulation, (16), at $N = 3$ [dotted black lines in Figs. 4(g) and 4(h)].

V. SELF-COMPRESSION OF ± SOLITONS IN ACTIVE MCFs

This section presents studies of self-compression of out-of-phase solitonlike laser pulses propagating in an active MCF [$G(\omega) \neq 0$] with a finite-gain bandwidth under the influence of Raman nonlinearity ($\mu \neq 0$). As noted above, the found stable nonlinear solution, (8), is determined by the $\pm$ mode in the transverse direction and has the form of an NSE soliton in the longitudinal direction.

To obtain analytical estimates, we use the variational approach, which is generalized to the case of description of the nonlinear propagation of wave packets in nonconservative systems with a Gaussian form of the gain profile $G(\omega)$ on the frequency, (7). This will reduce the partial differential equation to a closed system of ordinary differential equations for the characteristic parameters of a solitary laser pulse having a Gaussian form:

$$u_n = (-1)^n \sqrt{\frac{W/2N}{\sqrt{\pi}\tau_p}} e^{-\frac{(\tau-q)^2}{2\tau_p^2} + i\rho(\tau-q)^2 - i\varpi(\tau-q) + i\theta}. \qquad (27)$$

Here, the parameters τ_p, ρ, ϖ, θ, and q characterize the pulse duration, chirp, frequency, and phase of the wave field at the center of intensity of the packet, whose position is determined by $q(z)$.

Despite the complication due to the absence of Hamiltonianity in the active medium, the variational approach can be formulated for Eq. (6) too. At this, along with the Lagrangian of the conservative part,

$$\mathcal{L} = \sum_{n=1}^{2N} \int_{-\infty}^{+\infty} \left[\frac{i}{2}\left(u_n \frac{\partial u_n^*}{\partial z} - u_n^* \frac{\partial u_n}{\partial z} \right) - \frac{1}{2}|u_n|^4 + \left| \frac{\partial u_n}{\partial \tau} \right|^2 - \chi (u_n u_{n+1}^* + u_{n+1} u_n^*) \right] d\tau, \tag{28}$$

it is necessary to determine the dissipative function

$$\delta\mathcal{Q} = \sum_{n=1}^{2N} \int_{-\infty}^{+\infty} \frac{iG(\omega)}{2\pi} [u_n(\omega)\delta u_n(\omega)^* - u_n^*(\omega)\delta u_n(\omega)] d\omega + \mu \sum_{n=1}^{2N} \int_{-\infty}^{+\infty} \frac{\partial |u_n|^2}{\partial \tau} \delta |u_n|^2 d\tau. \tag{29}$$

Changing the parameters $a_j = \{W, \tau_p, q, \rho, \varpi, \theta\}$ of the distribution, (27), during the propagation of laser pulses is described by the Euler equations ($\dot{a}_j = da_j/dz$) [42]

$$\frac{d}{dz}\frac{\partial \overline{\mathcal{L}}}{\partial \dot{a}_j} - \frac{\partial \overline{\mathcal{L}}}{\partial a_j} = \int \left[\frac{\delta \mathcal{Q}}{\delta u_n} \frac{\partial u_n}{\partial a_j} + \text{c.c.} \right] d\tau, \tag{30}$$

where $\overline{\mathcal{L}}$ are the Lagrange functions, (28), calculated on the given distribution of the field, (27).

Taking the integrals on the right-hand side of (30), we arrive at the system of ordinary differential equations for the parameters of the wave field, (27),

$$\frac{dW}{dz} = \frac{2W\tau_p\Omega\gamma}{\sigma} e^{-\tau_p^2\varpi^2/\sigma^2}, \tag{31a}$$

$$\frac{d\tau_p}{dz} = 4\rho\tau_p - \frac{\tau_p^2\Omega\gamma}{\sigma^5}\left(4\tau_p^6\rho^2\Omega^2 - \tau_p^2\Omega^2 - 8\tau_p^6\rho^2\varpi^2 + 2\tau_p^2\varpi^2 + 16\tau_p^8\rho^4 - 1\right) e^{-\tau_p^2\varpi^2/\sigma^2}, \tag{31b}$$

$$\frac{d\rho}{dz} = \frac{1}{\tau_p^4} - 4\rho^2 - \frac{W/2N}{\sqrt{8\pi}\tau_p^3} - \frac{4\gamma\tau_p\rho\Omega}{\sigma^5}\left(\sigma^2 - 2\tau_p^2\varpi^2\right) e^{-\tau_p^2\varpi^2/\sigma^2}, \tag{31c}$$

$$\frac{d\varpi}{dz} = -\frac{\mu W/2N}{\sqrt{2\pi}\tau_p^3} - \frac{2\tau_p\varpi\Omega\gamma}{\sigma^3}\left(1 + 4\tau_p^4\rho^2\right) e^{-\tau_p^2\varpi^2/\sigma^2}, \tag{31d}$$

$$\frac{dq}{dz} = \frac{4\tau_p^5\rho\varpi\Omega\gamma}{\sigma^3} e^{-\tau_p^2\varpi^2/\sigma^2} - 2\varpi, \tag{31e}$$

where $\sigma = \sqrt{\tau_p^2\Omega^2 + 4\tau_p^4\rho^2 + 1}$. Equation (31e) for the velocity of the center of intensity of the wave packet is isolated from the rest of Eqs. (31).

The system of equations (31) is greatly simplified if injected laser pulses have a solitonlike form corresponding to the equilibrium state of Eqs. (31b) and (31c). This gives a relation between the energy W, the frequency modulation ρ, and the laser pulse duration τ_p:

$$W \approx 2N\frac{\sqrt{8\pi}}{\tau_p}, \quad \rho \simeq -\frac{\gamma}{4\tau_p^2\Omega^2}. \tag{32}$$

We assume that the frequency modulation is small on the scale of the wave packet $\rho\tau_p^2 \ll 1$. As a result, we obtain the following system of equations that determines the decrease in the duration τ_p and the shift of the center frequency ϖ down the spectrum of the wave packet of the soliton form:

$$\frac{d\tau_p}{dz} = -2\frac{\tau_p^2\Omega\gamma}{\sqrt{1+\tau_p^2\Omega^2}} e^{-\frac{\tau_p^2\varpi^2}{(1+\tau_p^2\Omega^2)^2}}, \tag{33a}$$

$$\frac{d\varpi}{dz} = -\frac{2\mu}{\tau_p^4} - \frac{2\varpi\Omega\gamma\tau_p}{(1+\tau_p^2\Omega^2)^{3/2}} e^{-\frac{\tau_p^2\varpi^2}{(1+\tau_p^2\Omega^2)^2}}. \tag{33b}$$

The phase planes of this system of equations are shown in Fig. 5.

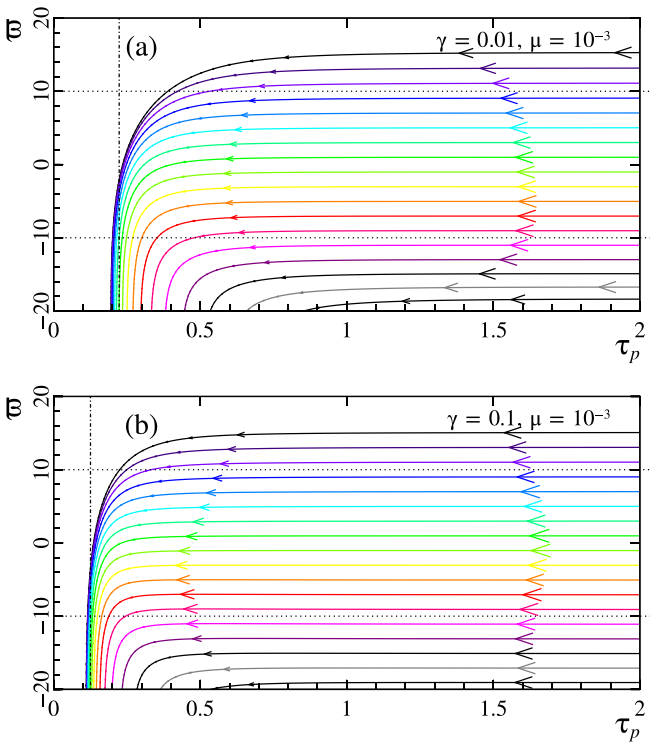

FIG. 5. Phase plane (τ_p, ϖ) of Eqs. (33) drawn for different values of the coefficients: (a) $\gamma = 0.01$, $\mu = 10^{-3}$; (b) $\gamma = 0.1$, $\mu = 10^{-3}$. The dashed vertical line represents the estimate of the minimum laser pulse duration, (38). Calculations were performed at $\Omega = 10$.

The nonstationarity of the nonlinear response leads to the appearance of the minimal duration τ_{lim}, to which the wave packet can be shortened during amplification. It follows from Fig. 5 that at the initial stage, when the Raman nonlinearity does not affect the wave-field dynamics, an adiabatic decrease in the wave-packet duration at a constant center frequency is realized. At the final stage, the Raman response stops the decrease in the duration of the laser pulse due to a significant shift of the wave-field spectrum to the long-wavelength region

and to further removal of the radiation spectrum from the gain band of the active medium $\varpi \gtrsim \Omega$. It can be seen (Fig. 5) that with a decrease in the gain γ at a constant value of the coefficient μ, an increase in the minimum value of the duration $\tau_{\rm lim}$ of the compressed laser pulse takes place.

Let us estimate the minimal duration $\tau_{\rm lim}$ depending on the parameters based on Eqs. (33). Let a laser pulse with the initial parameters be injected at the input of a nonlinear medium: $\tau_{\rm in}\Omega \gg 1$ and $\varpi_{\rm in} = 0$. As noted above, there is a decrease in the duration of the laser pulse at a practically constant frequency at the initial stage. So, Eq. (33a) reduces to

$$\frac{d\tau_p}{dz} \simeq -2\gamma\tau_p \tag{34}$$

and has the solution

$$\tau_p(z) = \tau_{\rm in}\exp(-2\gamma z). \tag{35}$$

At the final stage, the frequency of the wave packet shifts down the spectrum rapidly due to the nonstationary nonlinear response of the medium, in accordance with Eq. (33b):

$$\frac{d\varpi}{dz} \simeq -\frac{2\mu}{\tau_p^4}. \tag{36}$$

Substituting the expression for the wave-packet duration, (35), into Eq. (36), we find a solution for changing the carrier frequency:

$$\varpi(z) = -\frac{\mu}{4\gamma\tau_{\rm in}^4}\exp(8\gamma z) \equiv -\frac{\mu}{4\gamma\tau_p^4}. \tag{37}$$

The exponential decrease in the laser pulse duration will stop when the central radiation frequency is shifted beyond the medium gain band $|\varpi| \sim \Omega$. This gives an estimate of the minimal duration of the compressed laser pulse depending on the medium parameters:

$$\tau_{\rm lim} = \left(\frac{\mu}{4\gamma\Omega}\right)^{1/4}. \tag{38}$$

It can be seen from this expression that large gain values γ yield shorter wave-packet durations.

In Fig. 5, thedotted black line shows the position of the minimal duration $\tau_{\rm lim}$. The estimated value of $\tau_{\rm lim}$ is in good agreement with the results of a numerical analysis of the phase plane of Eqs. (31). Note that in the case where the carrier frequency of the injected wave packet is additionally shifted up the spectrum $\varpi_{\rm in} = \Omega$, the degree of compression of the laser pulse can be slightly increased, by approximately $\sqrt[4]{2} \approx 1.19$ times.

In dimensional variables, the compression length, the minimum duration, and the maximum laser pulse energy are

$$L_{\rm comp} = \frac{1}{2\gamma}\ln\frac{\tau_{\rm in}}{\tau_{\rm lim}} = \frac{1}{2\gamma}\ln\left[\tau_{\rm in}\sqrt[4]{\frac{8\gamma\Omega}{\tau_R\beta}}\right], \tag{39a}$$

$$\tau_{\rm lim} = \sqrt[4]{\frac{\tau_R\beta}{8\gamma\Omega}}, \tag{39b}$$

$$W_{\rm lim} = \frac{4\sqrt{\pi}N}{\Gamma}\sqrt[4]{\frac{2\beta^3\Omega\gamma}{\tau_R}}. \tag{39c}$$

Note that the wave-packet duration at half-maximum intensity is $\tau_{\rm lim}^{\rm FWHM} = 2\sqrt{\ln 2}\tau_{\rm lim}$.

Recall that the proposed method for decreasing the duration of the out-of-phase solitonlike laser pulse in the active MCF adiabatically is possible under applicability conditions (22), (23), and (24).

VI. NUMERICAL SIMULATIONS

To illustrate the proposed method of laser pulse self-compression, we turn to the results of numerical simulation within the framework of the initial equation, (2), with the nonlinear response $P_n^{\rm NL}$, (3). A laser pulse at the wavelength $\lambda = 2\ \mu$m with an initial duration of $\tau_{\rm in}^{\rm FWHM} = 1$ ps (half-height intensity) was injected into the input of a six-core silica MCF ($N = 3$) doped with thulium. The calculations were performed for a fiber with the following parameters: the group velocity dispersion $\beta = 100\ {\rm ps}^2/{\rm km}$, the nonlinearity coefficient $\Gamma = 1/({\rm W\ km})$, and the gain band $1/\Omega = 30$ fs [43].

Figure 6 shows the evolution of a laser pulse in a medium with the gain $\gamma^{-1} = 20$ m, which corresponds to the adiabatic mode of wave-packet amplification (the dispersion length is less than the gain length). A laser pulse was injected at the MCF input in the form of the found spatiotemporal soliton, (8),

$$E_n = (-1)^n\frac{17.54}{\cosh\left(\tau/\tau_{\rm sol}^{\rm in}\right)}, \tag{40}$$

where $|E_n|^2$ is measured in watts, and $\tau_{\rm sol}^{\rm in} = \frac{1}{2\,{\rm acosh}\sqrt{2}}\tau_{\rm in}^{\rm FWHM} = 0.57$ ps is the duration of the soliton. The dispersion length is $(\tau_{\rm sol}^{\rm in})^2/2\beta \approx 1.6$ m. This corresponds to an initial energy in the MCF with six cores, $W_{\rm in}^{6\ \rm cores} = 2.1$ nJ. From expressions (39) it follows that at the MCF output $L_{\rm comp} \approx 23$ m long, the wave-packet duration will reach the minimum value $\tau_{\rm lim}^{\rm FWHM} \approx 97$ fs. To ensure the regime of stable laser pulse propagation in the MCF, it is necessary to choose the coupling coefficient χ so that the coupling length is much less than the dispersion length, (23), estimated for the minimal duration $\tau_{\rm lim}^{\rm FWHM}$. This corresponds to the coupling coefficient $\chi^{-1} < 0.5$ cm.

Figure 6(a) shows the dynamics of the wave packet $E_n(z,\tau)$ and its spectrum [Fig. 6(b)] along the propagation path z. The electric-field strength and its spectrum are normalized to their maximum values. The horizontal dashed lines in Fig. 6(b) show the boundary of the gain band $\omega = -\Omega/2 = -17 \times 10^{12}\ {\rm s}^{-1}$. As shown in Fig. 6(a), the $\pm$ mode is preserved during the laser pulse evolution in the active MCF (the relative phase difference of the fields between neighboring nuclei is π). Figures 6(d) and 6(e) show the distribution of the total wave field $|\sum(-1)^n E_n(\tau)|$ and its spectrum distribution for different z. The dotted red line shows the initial distribution, the black line shows the current distribution, and the dashed vertical line shows the border of the gain band. At the initial stage ($z \lesssim 20$ m), as the wave packet propagates in the medium, an adiabatic decrease in the laser pulse duration takes place [see Fig. 6(a)]. At this, the spectrum broadens uniformly in both directions at a constant center frequency of the laser pulse [see Figs. 6(b) and 6(e) at $z = 10$ m].

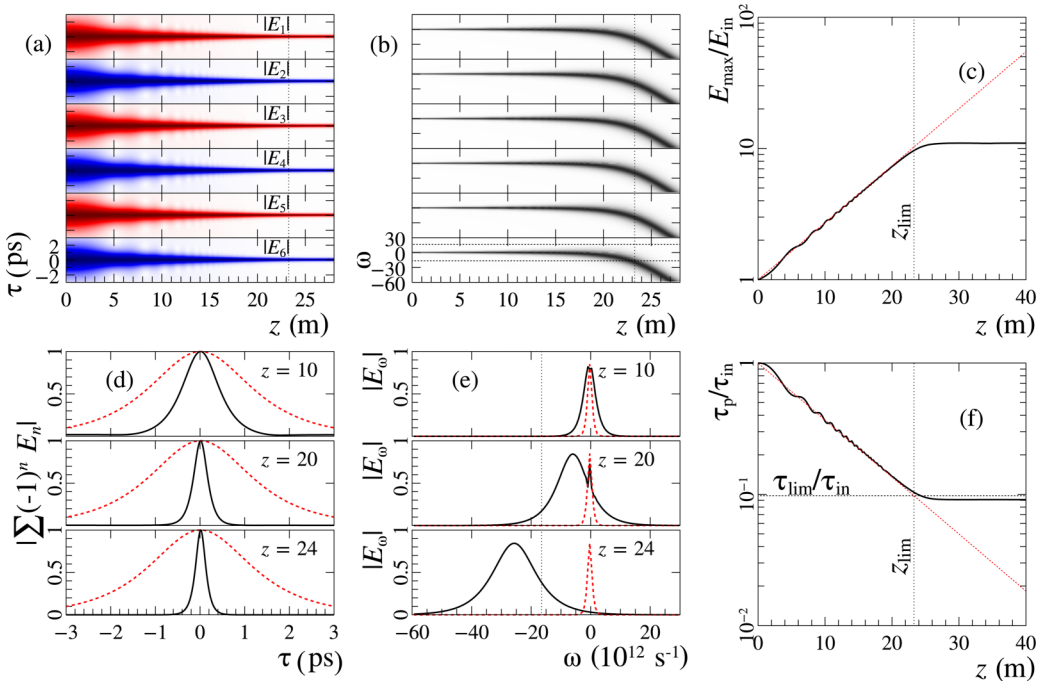

FIG. 6. Dynamics of the wave packet $E_n(z,\tau)$ (a) and its spectrum $E_n(z,\omega)$ (b) along the propagation path z (the electric-field strength and its spectrum are normalized to their maximal values), the maximal amplitude (c), and the laser pulse duration (f) depending on z. (d, e) Distribution of the total wave field $|\sum(-1)^n E_n(\tau)|$ and its spectrum for different z values. The dashed horizontal line in (f) shows the value, (39b). The dashed vertical line in (e) is the boundary of the gain band of the active medium, $\omega = -\Omega/2 = -17 \times 10^{12}$ s^{-1}. Dashed vertical lines in (a–c) and (f) are the medium length, $L_{comp} \approx 23$ m, at which the wave-packet duration reaches the minimal value, (39a), $\tau_{lim}^{FWHM} \approx 97$ fs. Calculations were performed for $\tau_{in}^{FWHM} = 1$ ps, $\beta = 100$ ps^2/km, $1/\gamma = 20$ m, $1/\Omega = 30$ fs, $\chi^{-1} = 3$ mm, and $\Gamma = 1$ (W km)$^{-1}$.

Subsequently, the spectrum of the wave field begins to shift to the long-wave part due to the influence of the nonstationary nonlinear response. The laser pulse spectrum goes beyond the gain band at $z \approx 24$ m [see Figs. 6(b) and 6(e)], and the decrease in the duration of the wave packet stops. Further, the center of the laser pulse spectrum monotonically shifts to the long-wavelength region for a constant duration of the wave packet [see Fig. 6(b)].

Figures 6(c) and 6(f) show the dependences of the maximum amplitude E_{max} [Fig. 6(c)] and the wave-packet duration τ_p [Fig. 6(d)] along the propagation path of z. Values are normalized to their initial values. The dotted red line shows the approximation of the laser pulse parameters $u_{max} \propto e^{2\gamma z}$, $\tau_p \propto e^{-2\gamma z}$. It can be seen that throughout the evolution of the wave packet in the MCF, the adiabatic decrease in the duration of the found spatiotemporal soliton, (8), is maintained. The vertical line in Figs. 6(c) and 6(f) shows the position of the estimated compression length L_{comp}, (39a), and the dashed horizontal line in Fig. 6(f) shows the position of the minimal duration τ_{lim}, (39b). It is shown that the maximum increase in the field amplitude and the maximum decrease in the duration of the laser pulse are achieved on the path $z \approx L_{comp}$. Subsequently, the considered quantities reach stationary values. Therefore, the obtained estimates of the minimal duration of the wave packet τ_{lim} and the compression length L_{comp} are in good agreement with the results of numerical simulation.

Thus, at the output of an active MCF of length $L_{comp} \approx 23$ m, the wave packet is shortened by about 10 times, from $\tau_{in}^{FWHM} = 1$ ps to $\tau_{out}^{FWHM} \approx 97$ fs, for the gain $\gamma^{-1} = 20$ m. However, implementation of such an extended active medium seems difficult. In this regard, we consider an MCF with a larger gain, $\gamma^{-1} = 2$ m. An increase in the value of the parameter γ by an order of magnitude should lead to a decrease in the compression length and to a decrease in the minimal wave-packet duration in comparison with the case $\gamma^{-1} = 20$ m, according to estimate (39).

Figure 7 shows the dynamics of the wave packet and its spectrum. Three stages of the evolution of a laser pulse can be distinguished here. The first stage is characterized by a noticeable discharge of radiation in the time domain [Fig. 7(a) at $z \lesssim 1.8$ m]. The reason is a violation of the adiabatic amplification condition for a soliton-shaped pulse (when the dispersion length is small with the gain length) for such a high value of the parameter γ. At this stage, the dependence of the maximum amplitude and minimum duration on the evolution variable z differs significantly from the exponential law $u_{max} \propto 1/\tau_p \propto e^{2\gamma z}$ [Figs. 7(c) and 7(f)]. A decrease in the laser pulse duration by several times leads to the second stage, where the pulse duration and maximum amplitude begin to change exponentially (quasiadiabatic regime), since at this stage the dispersion length becomes less than the gain length. At this stage, there is no radiation discharge. In accordance with the estimate, (39), the wave-packet duration reaches the minimal value of $\tau_{lim}^{FWHM} \approx 55$ fs at the MCF output $L_{comp} \approx 2.9$ m. Despite the initially nonadiabatic regime of amplification, the obtained estimates of the minimal laser pulse duration τ_{lim} and the compression length L_{comp} are in good agreement with the results of numerical simulation [Figs. 7(c) and 7(f)]. At the third stage ($z \gtrsim 3.2$ m), the duration of the

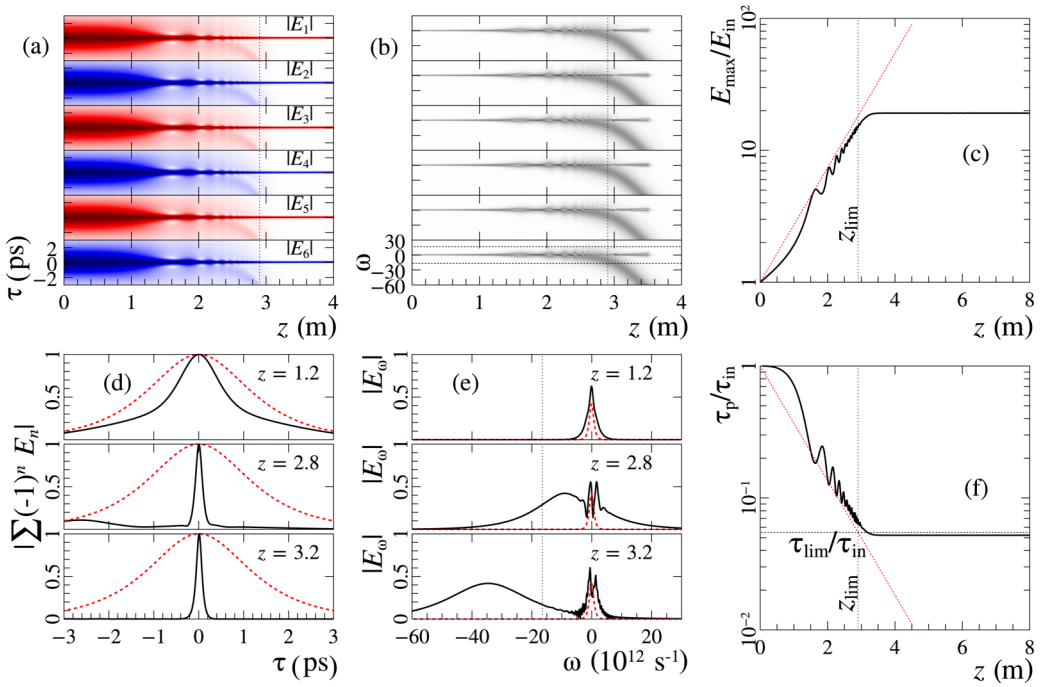

FIG. 7. Same as Fig. 6. Calculations were performed for $\tau_{\text{in}}^{\text{FWHM}} = 1$ ps, $\beta = 100$ ps^2/km, $1/\gamma = 2$ m, $1/\Omega = 30$ fs, $\chi^{-1} = 3$ mm, and $\Gamma = 1$ (W km)$^{-1}$. The dashed vertical line in (a–c) and (f) is the medium length, $L_{\text{comp}} \approx 2.9$ m, at which the wave-packet duration reaches the minimal value, (39a), $\tau_{\text{lim}}^{\text{FWHM}} \approx 55$ fs.

laser pulse does not change, since the spectrum of the laser pulse has shifted beyond the gain band.

It should be noted that due to the nonstationarity of the nonlinear response, the main signal is purified from the background radiation generated in the first stage due to the difference in group velocities. This is clearly shown in Fig. 7(d) at $z = 2.8$ m (the background radiation is located to the left of the main signal). Moreover, this difference in speeds increases with the growth of the z path, since the frequency of the main signal decreases as it propagates in media. As a result, the spatiotemporal soliton is purified of the background radiation quickly.

So, the performed qualitative analysis based on the variational approach is in good quantitative agreement with the results of numerical simulations performed within the framework of initial equation (2).

So, at the output of a 3-m-long MCF, it is possible to shorten the laser pulse from $\tau_{\text{in}}^{\text{FWHM}} = 1$ ps to $\tau_{\text{lim}}^{\text{FWHM}} \approx 55$ fs [Fig. 7(d)]. In this case, the energy contained in the spatiotemporal soliton at the output of a six-core MCF is $W_{\text{lim}}^{6\text{ cores}} \approx 38.4$ nJ (the energy in one core is $W_{\text{lim}}^{1\text{ core}} \approx 6.4$ nJ for these parameters). This energy can be significantly increased if one uses a large number of cores on the ring, $N \gg 1$. For example, in the case of 240 cores ($N = 120$), the energy in the laser pulse is $W_{\text{lim}}^{240\text{ cores}} = 1.5$ μJ. Unfortunately, the laser pulse compression in an MCF from such a large number of cores becomes sensitive to MCF deformations, (22), and gain inhomogeneities, (24), which contribute to the rescattering of the $\pm$ modes to other modes (see Sec. IV). As a result, the maximum achievable energy of the output wave packet in the proposed scheme is determined only by the technological capabilities of manufacturing an MCF with identical cores (see Table I). The gain homogeneity requirements $\frac{\delta\gamma}{\gamma} \ll \frac{2\chi}{\gamma}\frac{\pi^2}{N^2} \leqslant 1$ are significantly weaker due to the large factor, $2\chi/\gamma \sim 10^3$, for typical parameters $\chi^{-1} < 0.5$ cm, $\gamma^{-1} = 2$ m.

TABLE I. Maximal energy and requirements for δh for a different number of cores in the MCF.

No. of cores ($2N$)	W_{lim}	$\delta h/\chi$
6	$\approx$38.4 nJ	$\leqslant$1
20	$\approx$128 nJ	$\leqslant$0.1
60	$\approx$384 nJ	$\leqslant$0.01
200	$\approx$1.28 μJ	$\leqslant$0.001

VII. CONCLUSION

In this work we consider the propagation of out-of-phase wave packets in a multicore fiber (MCF) made of an even number of cores located in a ring. The exact nonlinear solution was found, (8), in the form of solitons with an out-of-phase distribution in the transverse direction. Its stability is proved with respect to both small perturbations of the wave field, including azimuthal ones, and small deformations of the MCF structure. The proof of the existence of a stable out-of-phase soliton opens up wide possibilities for its use as an analog of the fundamental mode for the considered MCFs, with the goal of significantly increasing the energy transported through MCFs and greatly exceeding the energy of the NSE soliton in a single core.

As an example of using this soliton distribution, we study the problem of compression of laser pulses in an active MCF with a sign-constant gain profile of a Gaussian form. The

qualitative analysis of the wave-packet self-action in the considered MCF is carried out based on the variational approach. The optimal fiber parameters, the minimal duration of the output pulse, and the compression length are found and are in good agreement with the results of numerical simulation. The requirements for MCF deformations and for the gain magnitude and uniformity are determined in order to achieve high energies in the output laser pulse.

ACKNOWLEDGMENT

This work was supported by Russian Science Foundation Grant No. 16-12-10472.

[1] G. Mourou, T. Tajima, M. N. Quinnb, B. Brocklesbyc, and J. Limpertd, Nucl. Instrum. Methods Phys. Res. A **740**, 17 (2014).
[2] G. Mourou, B. Brocklesby, T. Tajima, and J. Limpert, Nat. Photonics **7**, 258 (2013).
[3] M. Müller, M. Kienel, A. Klenke, T. Gottschall, E. Shestaev, M. Plötner, J. Limpert, and A. Tünnermann, Opt. Lett. **41**, 3439 (2016).
[4] J. Bourderionnet, C. Bellanger, J. Primot, and A. Brignon, Opt. Exp. **19**, 17053 (2011).
[5] A. Klenke, M. Müller, H. Stark, M. Kienel, C. Jauregui, A. Tünnermann, and J. Limpert, IEEE J. Select. Topics Quantum Electron. **24**, 0902709 (2018).
[6] A. A. Balakin, A. G. Litvak, V. A. Mironov, and S. A. Skobelev, Phys. Rev. A **94**, 063806 (2016).
[7] Y. S. Kivshar and S. K. Turitsyn, Phys. Rev. E **49**, R2536(R) (1994).
[8] A. B. Aceves, G. G. Luther, C. De Angelis, A. M. Rubenchik, and S. K. Turitsyn, Phys. Rev. Lett. **75**, 73 (1995).
[9] H. S. Eisenberg, Y. Silberberg, R. Morandotti, A. R. Boyd, and J. S. Aitchison, Phys. Rev. Lett. **81**, 3383 (1998).
[10] A. A. Balakin, A. G. Litvak, V. A. Mironov, and S. A. Skobelev, Laser Phys. **28**, 045401 (2018).
[11] T. X. Tran, D. C. Duong, and F. Biancalana, Phys. Rev. A **89**, 013826 (2014).
[12] P. Panagiotopoulos, P. Whalen, M. Kolesik, and J. V. Moloney, Nat. Photonics **9**, 543 (2015).
[13] T. X. Tran, D. C. Duong, and F. Biancalana, Phys. Rev. A **90**, 023857 (2014).
[14] D. Cheskis, S. Bar-Ad, R. Morandotti, J. S. Aitchison, H. S. Eisenberg, Y. Silberberg, and D. Ross, Phys. Rev. Lett. **91**, 223901 (2003).
[15] H. S. Eisenberg, R. Morandotti, Y. Silberberg, S. Bar-Ad, D. Ross, and J. S. Aitchison, Phys. Rev. Lett. **87**, 043902 (2001).
[16] A. A. Balakin, A. G. Litvak, V. A. Mironov, S. A. Skobelev, and L. A. Smirnov, Laser Phys. **28**, 105401 (2018).
[17] I. S. Chekhovskoy, A. M. Rubenchik, O. V. Shtyrina, M. P. Fedoruk, and S. K. Turitsyn, Phys. Rev. A **94**, 043848 (2016).
[18] A. M. Rubenchik, I. S. Chekhovskoy, M. P. Fedoruk, O. V. Shtyrina, and S. K. Turitsyn, Opt. Lett. **40**, 721 (2015).
[19] A. V. Andrianov, N. A. Kalinin, M. Yu. Koptev, O. N. Egorova, A. V. Kim, and A. G. Litvak, Opt. Lett. **44**, 303 (2019).
[20] A. M. Rubenchik, E. V. Tkachenko, M. P. Fedoruk, and S. K. Turitsyn, Opt. Lett. **38**, 4232 (2013).
[21] S. K. Turitsyn, A. M. Rubenchik, M. P. Fedoruk, and E. Tkachenko, Phys. Rev. A **86**, 031804(R) (2012).
[22] A. A. Balakin, S. A. Skobelev, E. A. Anashkina, A. V. Andrianov, and A. G. Litvak, Phys. Rev. A **98**, 043857 (2018).
[23] D. N. Christodoulides and R. I. Joseph, Opt. Lett. **13**, 794 (1988).
[24] B. A. Malomed, *Soliton Management in Periodic Systems* (Springer, Berlin, 2006).
[25] F. Lederer, G. I. Stegeman, D. N. Christodoulides, G. Assanto, M. Segev, and Y. Silberberg, Phys. Rep. **463**, 1 (2008).
[26] D. N. Christodoulides, F. Lederer, and Y. Silberberg, Nature **424**, 817 (2003).
[27] F. Eilenberger, S. Minardi, A. Szameit, U. Röpke, J. Kobelke, K. Schuster, H. Bartelt, S. Nolte, L. Torner, F. Ledere, A. Tünnermann, and T. Pertsch, Phys. Rev. A **84**, 013836 (2011).
[28] A. B. Aceves, O. V. Shtyrina, A. M. Rubenchik, M. P. Fedoruk, and S. K. Turitsyn, Phys. Rev. A **91**, 033810 (2015).
[29] S. Minardi, F. Eilenberger, Y. V. Kartashov, A. Szameit, U. Ropke, J. Kobelke, K. Schuster, H. Bartelt, S. Nolte, L. Torner, F. Lederer, A. Tunnermann, and T. Pertsch, Phys. Rev. Lett. **105**, 263901 (2010).
[30] D. Mihalache, D. Mazilu, F. Lederer, Y. V. Kartashov, L.-C. Crasovan, and L. Torner, Phys. Rev. E **70**, 055603(R) (2004).
[31] Y. V. Kartashov, C. Hang, G. Huang, and L. Torner, Optica **3**, 1048 (2016).
[32] H. Leblond, D. Kremer, and D. Mihalache, Phys. Rev. A **95**, 043839 (2017).
[33] L. F. Mollenauer, R. H. Stolen, J. P. Gordon, and W. J. Tomlinson, Opt. Lett. **8**, 289 (1983).
[34] Q. Li, J. N. Kutz, and P. K. A. Wai, JOSA B **27**, 2180 (2010).
[35] G. Agrawal, *Nonlinear Fiber Optics* (Academic Press, London, 2013).
[36] S. V. Chernikov, D. J. Richardson, E. M. Dianov, and D. N. Payne, Electron. Lett. **28**, 1842 (1992).
[37] M. L. Quiroga-Teixeiro, D. Anderson, P. A. Andrekson, A. Berntson, and M. Lisak, Opt. Soc. Am. B **13**, 687 (1996).
[38] M. Nakazawa, K. Kurokawa, H. Kubota, and E. Yamada, Phys. Rev. Lett. **65**, 1881 (1990).
[39] Y. S. Kivshar and G. Agrawal, *Optical Solitons: From Fibers to Photonic Crystals* (Academic Press, London, 2006).
[40] G. P. Agrawal, IEEE Photon. Tech. Lett. **2**, 875 (1990).
[41] L. W. Liou and G. P. Agrawal, Opt. Commun. **124**, 500 (1996).
[42] A. Ankiewicz, N. Akhmediev, and N. Devine, Opt. Fiber Technol. **13**, 91 (2007).
[43] S. D. Jackson and T. A. King, J. Lightwave Technol. **17**, 948 (1999).